Effects of inclusion shapes on the band gaps in two-dimensional piezoelectric phononic crystals

2007 J. Phys.: Condens. Matter 19 496204

(http://iopscience.iop.org/0953-8984/19/49/496204)

IOP PUBLISHING JOURNAL OF PHYSICS: CONDENSED MATTER

J. Phys.: Condens. Matter **19** (2007) 496204 (9pp) doi:10.1088/0953-8984/19/49/496204

Effects of inclusion shapes on the band gaps in two-dimensional piezoelectric phononic crystals

Yi-Ze Wang[1], Feng-Ming Li[1,3], Wen-Hu Huang[1] and Yue-Sheng Wang[2]

[1] School of Astronautics, Harbin Institute of Technology, PO Box 137, Harbin 150001, People's Republic of China
[2] Institute of Engineering Mechanics, Beijing Jiaotong University, Beijing 100044, People's Republic of China

E-mail: fmli@hit.edu.cn

Received 13 July 2007, in final form 18 October 2007
Published 12 November 2007
Online at stacks.iop.org/JPhysCM/19/496204

Abstract

In this paper, the elastic wave propagation in piezoelectric phononic crystals with several inclusion shapes is investigated by taking the electromechanical coupling into account. The band structures for five different shapes of scatterers (regular triangle, square, hexagon, circle, and oval) with square lattice are calculated using the plane-wave expansion method. The effects of the inclusion shapes on the normalized band width are discussed. The largest complete band gap is obtained by selecting the scatterers with the same symmetry of lattice for the first band gap, but this rule is not valid for the second band gap.

1. Introduction

During the past few years, much effort has been devoted to the research of elastic wave propagation in periodic composite materials, which are called phononic crystals with the property of elastic wave band gap [1–4]. In the complete band gaps, the propagation is forbidden for all wavevectors. With these characteristics, such structures have many potential applications such as acoustic transducers and filters and vibration isolation technology.

Among various types of phononic crystals, piezoelectric ones, which have superior electric effects, have recently received increasing attention. It should be pointed out that Khelif and his co-workers used the plane-wave expansion (PWE) method to investigate a series of problems on the piezoelectric phononic crystals and drew some important conclusions [5–7]. Hou *et al* employed a similar procedure to analyze the effects of piezoelectricity on the band gaps [8]. Wu *et al* applied the same method to study the electromechanical coupling coefficient of surface waves in two-dimensional piezoelectric phononic crystals [9]. Li *et al* studied the wave

[3] Author to whom any correspondence should be addressed.

0953-8984/07/496204+09$30.00

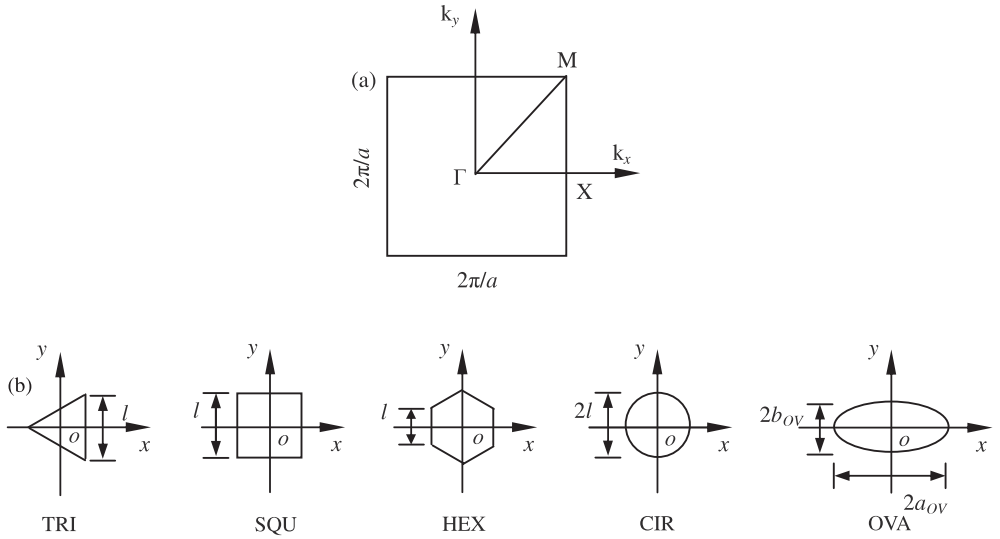

Figure 1. (a) The first irreducible Brillouin zone of the square lattice for two-dimensional phononic crystals with piezoelectric phase. (b) The considered inclusion shapes and their dimensions.

propagation and localization in disordered layered piezoelectric phononic crystals taking the electromechanical coupling into account [10, 11].

It is well known that the inclusion shapes play an important role in the band gaps, which has been studied by Villeneuve and Piché for a similar problem in photonic crystals [12–14]. However, to our knowledge, there is no research on the effects of inclusion shapes for piezoelectric phononic crystals. In our opinion, by considering the mechanical and electrical coupling, some new phenomena can be found in this new type of structure. In this paper, the effects of five different shapes of piezoelectric inclusions (i.e. regular triangle, square, hexagon, circle, and oval) on the wave band gaps are studied using the plane-wave expansion method. The relation between the normalized mid-gap frequency and scatter shapes for both the first and second band gaps are discussed and some significant conclusions are drawn.

2. Equations of wave motion

We consider two-dimensional piezoelectric phononic crystals with square lattice. The lattice constant is a. Figure 1 shows the corresponding first irreducible Brillouin zone and the five kinds of inclusion shapes.

The constitutive equations of piezoelectric materials are given by

$$\begin{aligned} \sigma_{ij} &= c_{ijmn}\,\varepsilon_{mn} - e_{nij}E_n, \\ D_i &= e_{imn}\,\varepsilon_{mn} + \epsilon_{in}E_n, \qquad (i, j, m, n = 1, 2, 3), \end{aligned} \tag{1}$$

where σ_{ij} is the elastic stress tensor, D_i the electric displacement vector, ε_{mn} the elastic strain tensor, E_n the electric field intensity, $c_{ijmn}(\boldsymbol{r})$ the elastic constant, $e_{nij}(\boldsymbol{r})$ the piezoelectric constant, and $\epsilon_{in}(\boldsymbol{r})$ the dielectric constant, which are all position-dependent material constants. $\boldsymbol{r} = (x, y)$ is the position vector. In equation (1), the summation convention is employed. Because the phononic crystals are homogeneous along the z axis, these constants are independent of the coordinate z.

The elastic strain tensor ε_{mn} and electric field intensity E_n can be expressed in the following forms:

$$\varepsilon_{mn} = \tfrac{1}{2}(u_{m,n} + u_{n,m}), \qquad E_n = -\frac{\partial \varphi}{\partial x_n} = -\varphi_{,n}, \tag{2}$$

where $u_m = \{u_x, u_y, u_z\}^{\mathrm{T}}$ is the elastic displacement vector and φ is the electric potential.

The differential equation of the motion in the absence of body forces is given by

$$\sigma_{ij,j} = \rho \ddot{u}_i, \qquad D_{i,i} = 0, \tag{3}$$

where $\rho(\boldsymbol{r})$ is the mass density of the materials which is also position-dependent and the dot denotes differentiation with respect to time.

Based on the Bloch theorem, the displacement vector $u_i(\boldsymbol{r}, t)$ and electric potential φ can be expanded in Fourier series:

$$\begin{aligned} u_i(\boldsymbol{r}, t) &= \sum_G u^i_{k+G} \exp[\mathrm{i}(\boldsymbol{k}\cdot\boldsymbol{r} + \boldsymbol{G}\cdot\boldsymbol{r} - \omega t)], \\ \boldsymbol{\varphi}(\boldsymbol{r}, t) &= \sum_G \boldsymbol{\varphi}_{k+G} \exp[\mathrm{i}(\boldsymbol{k}\cdot\boldsymbol{r} + \boldsymbol{G}\cdot\boldsymbol{r} - \omega t)], \end{aligned} \tag{4}$$

where $\boldsymbol{k} = (k_x, k_y)$ is the Bloch wavevector, ω the circular frequency, and u^i_{k+G} and $\boldsymbol{\varphi}_{k+G}$ the amplitudes of the displacement vectors and electric potential. In practical problems, it is essential to assume a truncation N of the plane wavenumber.

According to the periodicity of the structure, the material constants, $\rho(\boldsymbol{r})$, $c_{ijmn}(\boldsymbol{r})$, $e_{nij}(\boldsymbol{r})$, and $\epsilon_{in}(\boldsymbol{r})$ can be expanded in the Fourier series

$$\alpha(\boldsymbol{r}) = \sum_G \alpha_G \exp(\mathrm{i}\boldsymbol{G}\cdot\boldsymbol{r}), \tag{5}$$

where $\boldsymbol{G} = (-2\pi M/a, 2\pi M/a)$ is the two-dimensional reciprocal lattice vector with integer M, α is either one of ρ, c_{ijmn}, e_{nij}, or ϵ_{in}, and α_G is either one of ρ_G, c^{ijmn}_G, e^{nij}_G, or ϵ^{in}_G, which are the corresponding Fourier coefficients of the material constants. The expression of α_G is

$$\alpha_G = S^{-1} \int_S \mathrm{d}^2 r \alpha(\boldsymbol{r}) \exp(-\mathrm{i}\boldsymbol{G}\cdot\boldsymbol{r}), \tag{6}$$

where S is the area of one unit cell of the lattice. The integral in equation (6) can be simplified as follows:

$$\alpha_G = \begin{cases} \alpha_A f + \alpha_B(1-f) & \text{for } \boldsymbol{G} = 0 \\ (\alpha_A - \alpha_B) F_G & \text{for } \boldsymbol{G} \neq 0, \end{cases} \tag{7}$$

where α_A and α_B denote the material constants of the inclusion phase and the matrix medium, respectively, and $f = S_A/S$ is the filling fraction ratio of the inclusion, where S_A is the area of the inclusion within a unit cell of the lattice. The structure function F_G is defined by

$$F_G = S^{-1} \int_{S_A} \mathrm{d}^2 r \exp(-\mathrm{i}\boldsymbol{G}\cdot\boldsymbol{r}). \tag{8}$$

3. Expressions of structure function and the generalized eigenvalue equation

For the regular triangle, square, hexagon, circle, and oval scatterers shown in figure 1, F_G is denoted by F^{t}_G, F^{s}_G, F^{h}_G, F^{c}_G, or F^{o}_G, respectively. The results of equation (8) are

expressed in [15–17]:

(A) *Regular triangle*

$$
\begin{aligned}
\mathrm{Re}\, F^{\mathrm{t}}_{Gx,0} &= \frac{1}{3SG_x^2}\left[3lG_x \sin\left(\frac{\sqrt{3}lG_x}{6}\right) + 2\sqrt{3}\cos\left(\frac{\sqrt{3}lG_x}{6}\right) - 2\sqrt{3}\cos\left(\frac{\sqrt{3}lG_x}{3}\right)\right],\\
\mathrm{Im}\, F^{\mathrm{t}}_{Gx,0} &= \frac{1}{3SG_x^2}\left[3lG_x \cos\left(\frac{\sqrt{3}lG_x}{6}\right) - 2\sqrt{3}\sin\left(\frac{\sqrt{3}lG_x}{6}\right) - 2\sqrt{3}\sin\left(\frac{\sqrt{3}lG_x}{3}\right)\right],\\
\mathrm{Re}\, F^{\mathrm{t}}_{Gx,\pm\sqrt{3}Gx} &= \frac{1}{6SG_x^2}\left[\sqrt{3}\cos\left(\frac{\sqrt{3}lG_x}{3}\right) - \sqrt{3}\cos\left(\frac{2\sqrt{3}lG_x}{3}\right)\right.\\
&\quad \left. + 3lG_x \sin\left(\frac{\sqrt{3}lG_x}{3}\right)\right],\\
\mathrm{Im}\, F^{\mathrm{t}}_{Gx,\pm\sqrt{3}Gx} &= \frac{1}{6SG_x^2}\left[\sqrt{3}\sin\left(\frac{\sqrt{3}lG_x}{3}\right) + \sqrt{3}\sin\left(\frac{2\sqrt{3}lG_x}{3}\right)\right.\\
&\quad \left. - 3lG_x \cos\left(\frac{\sqrt{3}lG_x}{3}\right)\right],\\
\mathrm{Re}\, F^{\mathrm{t}}_{Gx,Gy} &= \frac{1}{SG_y(3G_x^2 - G_y^2)}\left[6G_x \sin\left(\frac{\sqrt{3}lG_x}{6}\right)\sin\left(\frac{lG_y}{2}\right)\right.\\
&\quad \left. + 2\sqrt{3}G_y \cos\left(\frac{\sqrt{3}lG_x}{6}\right)\cos\left(\frac{lG_y}{2}\right) - 2\sqrt{3}G_y \cos\left(\frac{\sqrt{3}lG_x}{3}\right)\right],\\
\mathrm{Im}\, F^{\mathrm{t}}_{Gx,Gy} &= \frac{1}{SG_y(3G_x^2 - G_y^2)}\left[6G_x \cos\left(\frac{\sqrt{3}lG_x}{6}\right)\sin\left(\frac{lG_y}{2}\right)\right.\\
&\quad \left. - 2\sqrt{3}G_y \sin\left(\frac{\sqrt{3}lG_x}{6}\right)\cos\left(\frac{lG_y}{2}\right) - 2\sqrt{3}G_y \sin\left(\frac{\sqrt{3}lG_x}{3}\right)\right],
\end{aligned}
\tag{9}
$$

where Re and Im are the real and imaginary parts of F^{t}_G and G_x and G_y are the x and y components of $\boldsymbol{G}$.

(B) *Square*

$$
\begin{aligned}
F^{\mathrm{s}}_{Gx,0} &= \frac{2l}{SG_x}\sin\left(\frac{G_x l}{2}\right), \qquad F^{\mathrm{s}}_{0,Gy} = \frac{2l}{SG_y}\sin\left(\frac{G_y l}{2}\right),\\
F^{\mathrm{s}}_{Gx,Gy} &= \frac{4}{SG_xG_y}\sin\left(\frac{G_x l}{2}\right)\sin\left(\frac{G_y l}{2}\right).
\end{aligned}
\tag{10}
$$

(C) *Hexagon*

$$
\begin{aligned}
F^{\mathrm{h}}_{Gx,0} &= \frac{2f}{3G_x l}\left[\sin(G_x l) + \frac{1-\cos(G_x l)}{G_x l}\right],\\
F^{\mathrm{h}}_{Gx,\pm\sqrt{3}Gx} &= \frac{f}{3G_x l}\left[\sin(2G_x l) + \frac{1-\cos(2G_x l)}{2G_x l}\right],\\
F^{\mathrm{h}}_{Gx,Gy} &= \frac{f}{G_y l}\left[\frac{\cos(G_y l/\sqrt{3} - G_x l) - \cos(2G_y l/\sqrt{3})}{(G_y + \sqrt{3}G_x)l}\right.\\
&\quad \left. + \frac{\cos(G_y l/\sqrt{3} + G_x l) - \cos(2G_y l/\sqrt{3})}{(G_y - \sqrt{3}G_x)l}\right].
\end{aligned}
\tag{11}
$$

(D) *Circle*

$$
F^{\mathrm{c}}_G = \frac{2fJ_1(Gl)}{Gl},
\tag{12}
$$

Table 1. Material constants of $BaTiO_3$ and polymer.

	Mass density (10^3 kg m^{-3})	Elastic constant (10^9 N m^{-2})				Piezoelectric constant (C m^{-2})			Piezoelectric constant (10^{-9} C^2 N^{-1} m^{-2})	
Materials	ρ	c_{11}	c_{12}	c_{44}	c_{66}	e_{13}	e_{15}	e_{33}	ϵ_{11}	ϵ_{33}
$BaTiO_3$	5.8	166	77	43	44.5	−4.4	11.6	18.6	11.2	12.6
Polymer	1.15	7.8	4.7	1.6	1.55	0	0	0	0.0398	0.0398

where $J_1(\cdot)$ is the Bessel function of the first kind of order one.

(E) *Oval*

$$F_G^{\mathrm{o}} = \frac{2fJ_1(G'b_{\mathrm{ov}})}{G'b_{\mathrm{ov}}}, \tag{13}$$

where $G'_x = G_x a_{\mathrm{ov}}/b_{\mathrm{ov}}$, $G'_y = G_y$ and a_{ov} and b_{ov} are the lengths of the long and short half axes.

Substituting equations (1), (2), (4), and (5) into equation (3), we obtain the following generalized eigenvalue equation in the matrix form

$$\boldsymbol{\omega}^2 \boldsymbol{R}\boldsymbol{U} = \boldsymbol{Q}\boldsymbol{U}, \tag{14}$$

where $\boldsymbol{U} = \{u_G^x, u_G^y, u_G^z, \boldsymbol{\varphi}_G\}^{\mathrm{T}}$ is the generalized displacement vector, $\boldsymbol{R}$ and $\boldsymbol{Q}$ the $4N \times 4N$ matrices which are functions of $\boldsymbol{k}$, and $\boldsymbol{G}$ and $\boldsymbol{G}'$ the Fourier coefficients of the material constants. The elements of matrices $\boldsymbol{R}$ and $\boldsymbol{Q}$ are listed in the appendix. It should be noted that the *xy*-mode and *z*-mode are decoupled.

4. Numerical results and discussion

In this section, numerical computation for the piezoelectric phononic crystals—$BaTiO_3$/polymer—is performed. The material constants used in the calculation are listed in table 1.

For the five types of piezoelectric phononic structures mentioned above, figures 2–4 show the band structures in the first Brillouin zone for the symmetry axis with $b_{\mathrm{ov}}/a_{\mathrm{ov}} = 0.8$ for the oval rods. The filling fraction $f = S_A/S$ is taken as 0.35. For the normalized frequency $\omega a/2\pi c_{\mathrm{t}}$, c_{t} is the velocity of transverse waves in the polymer. The *xy*-mode and *z*-mode are shown by the solid and dashed lines and the gray zones denote the complete band gaps for elastic waves.

It can be observed that the band structures change pronouncedly for different cases. For the regular triangle rods presented in figure 2(a), a third complete band gap exists but not in other types. The second band gap is wider than the first one in figure 2(a). However, for the square scatterers in figure 2(b), the case is just the opposite. The first band gap is much wider not only than the second one but also than that of the regular triangle case. It should be noted that the first band gap is wider and the contrast of the width between the first and second gaps is more apparent for square inclusions than the other cases which are displayed in figures 2–4.

Moreover, from figures 3(a) and (b), it can be seen that the contrast of the width between the first and second gaps in each case is not apparent. However, the contrast is obvious for the first gaps between figures 3(a) and (b) and the same as the second gaps. The positions of the band gaps for hexagon and circle cases are different. The corresponding gaps are higher in figure 3(a) than those of figure 3(b). It means that the elastic waves propagating freely for the hexagon case may be stopped for the circle case.

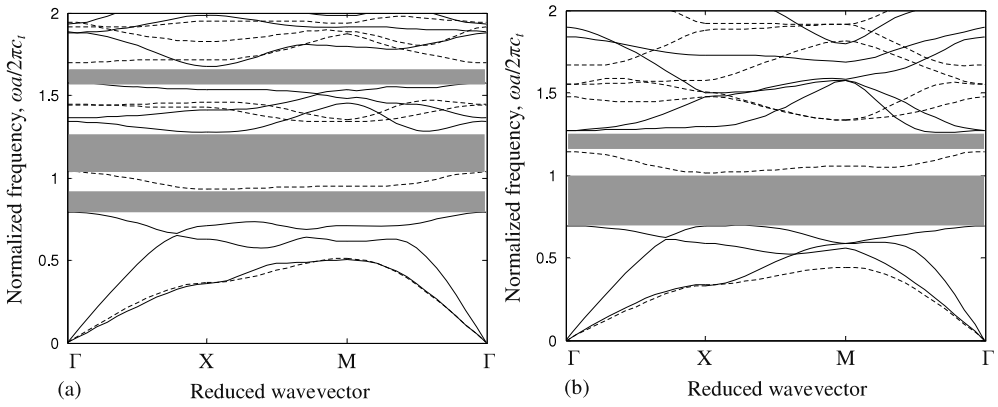

Figure 2. The band structures of two-dimensional piezoelectric phononic crystals with $f = 0.35$: (a) for regular triangle inclusions and (b) for square inclusions. The gray regions denote complete band gaps. The solid and dashed lines denote the *xoy* mode and *z* mode.

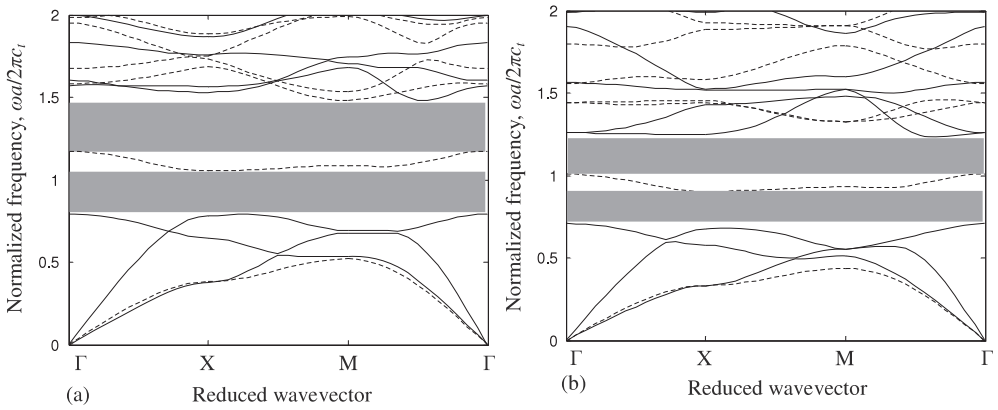

Figure 3. The band structures of two-dimensional piezoelectric phononic crystals with $f = 0.35$: (a) for hexagon inclusions and (b) for circle inclusions. The gray regions denote complete band gaps. The solid and dashed lines denote the *xoy* mode and *z* mode.

The most prominent feature in figure 4 is that, although there is little difference of the width between the first and second band gaps just like figures 3(a) and (b), they are narrower than the two cases in figure 3. In other words, the band gap properties for this kind of piezoelectric phononic crystals have less superiority.

In order to analyze the effects of inclusion shapes on the band gap, the normalized band gap widths, $\Delta\omega/\omega_g$, are computed for different ratios f, where $\Delta\omega$ is the band gap width and ω_g is the normalized mid-gap frequency. The results for the first and second band gaps are illustrated in figures 5 and 6.

From figure 5, we can clearly observe that the widths of band gaps are changed by altering the shapes of the scatterers. For both the square and circle scatterers, the values increase with increase of filling fraction ratio f. However, for regular triangle, hexagon, and oval inclusions, the curves firstly increase and then decrease. Especially for regular triangle rods, the normalized gap width becomes zero when f reaches 0.475.

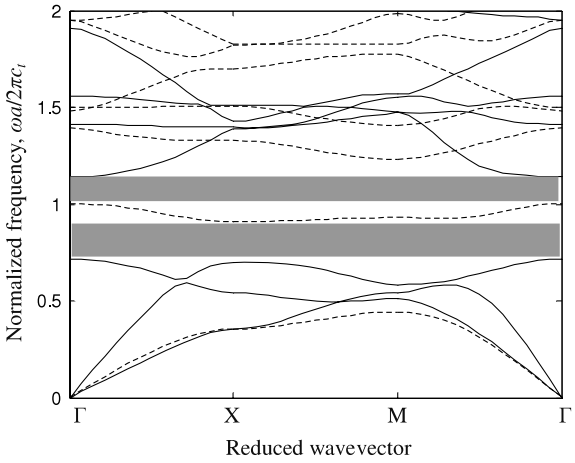

Figure 4. The band structures of two-dimensional piezoelectric phononic crystals with $f = 0.35$ for oval with $b_{ov}/a_{ov} = 0.8$ only. The gray regions denote complete band gaps. The solid and dashed lines denote the *xoy* mode and *z* mode.

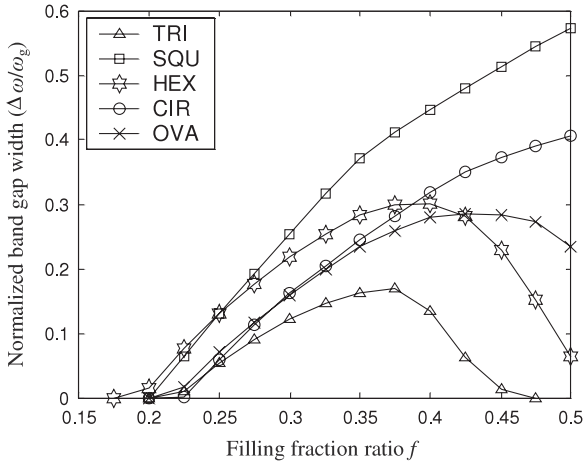

Figure 5. The normalized widths of the first complete band gaps as a function of the filling fraction ratio f for five different inclusions.

Another important feature in figure 5 is that in the considered regions the normalized gap width for the square rods is larger than any other kind of geometric shape. The reason is that the symmetry of rods is the same as the lattice geometry, which is similar to the case of photonic crystals investigated by Wang *et al* [15] and steel/air systems studied by Zhong *et al* [17]. This is why the first band gap in figure 2(b) is larger than the other four shapes for $f = 0.35$.

The most noticeable feature in figure 6 is that the normalized band gap width for square rods is the smallest among the considered five types and it does not change remarkably with f increasing. Both of the features in figure 6 are very different from those in figure 5, which does not obey the rule that the band gap width is the largest when the inclusion symmetry is the same as that of the lattice. So this rule is not valid in all the considered frequency regions for the second complete band gap. It can also be seen that for the case of oval scatterers the value of $\Delta\omega/\omega_g$ increases with f increasing unlike the curves in figure 5. The curves for both hexagon

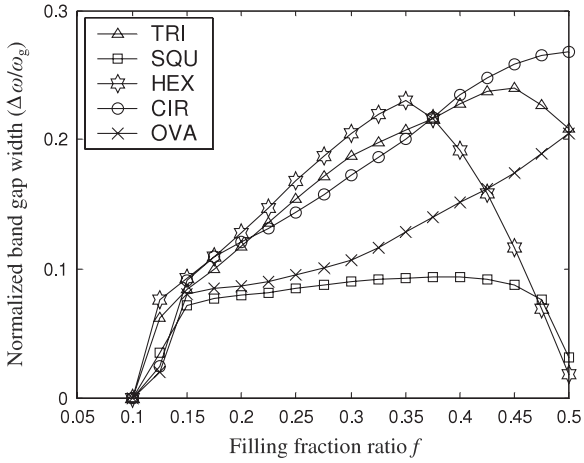

Figure 6. The normalized widths of the second complete band gaps as a function of the filling fraction ratio f for five different inclusions.

and circle cases in figure 6 are similar to those in figure 5, which means that the properties do not change obviously between the first and second band gaps.

5. Conclusions

In this paper, the plane-wave expansion method is used to study the elastic wave band gaps of piezoelectric phononic crystals with square lattice for regular triangle, square, hexagon, circle, and oval inclusions, respectively. The band gaps for the five cases are calculated. The effects of the inclusion shapes are discussed. From the results, the following conclusions can be drawn:

(1) There is a third complete band gap for the regular triangle rods, but not in the other cases.
(2) For the case of $f = 0.35$, the first band gap for square inclusions is the largest and the second one is the smallest among the considered five cases.
(3) The locations of band gaps for hexagon and circle rods are quite different from each other. Both the first and second band gaps are very narrow for the oval scatterers.
(4) When the shape symmetry of the inclusions is identical to the lattice, the largest complete band gap is obtained for the first band gap. But this rule is not valid for the second band gap.

Acknowledgment

The authors express gratitude for the support provided by the National Natural Science Foundation of China under grant nos 10672017 and 10632020 for this research work.

Appendix

The elements of matrices $\boldsymbol{R}$ and $\boldsymbol{Q}$ in equation (14) are expressed as:

$$\boldsymbol{R}_{G,G'} = \begin{bmatrix} \rho_{G-G'} & & & \\ & \rho_{G-G'} & & \\ & & \rho_{G-G'} & \\ & & & 0 \end{bmatrix}, \tag{A.1}$$

$$\boldsymbol{Q}_{G,G'} = \begin{bmatrix} \boldsymbol{Q}^{(1,1)}_{G,G'} & \boldsymbol{Q}^{(1,2)}_{G,G'} & \mathbf{0} & \mathbf{0} \\ \boldsymbol{Q}^{(2,1)}_{G,G'} & \boldsymbol{Q}^{(2,2)}_{G,G'} & \mathbf{0} & \mathbf{0} \\ \mathbf{0} & \mathbf{0} & \boldsymbol{Q}^{(3,3)}_{G,G'} & \boldsymbol{Q}^{(3,4)}_{G,G'} \\ \mathbf{0} & \mathbf{0} & \boldsymbol{Q}^{(4,3)}_{G,G'} & \boldsymbol{Q}^{(4,4)}_{G,G'} \end{bmatrix}, \tag{A.2}$$

where

$$\boldsymbol{Q}^{(1,1)}_{G,G'} = c^{11}_{G-G'}(\boldsymbol{k}+\boldsymbol{G})_1(\boldsymbol{k}+\boldsymbol{G}')_1 + c^{66}_{G-G'}(\boldsymbol{k}+\boldsymbol{G})_2(\boldsymbol{k}+\boldsymbol{G}')_2, \tag{A.3}$$

$$\boldsymbol{Q}^{(1,2)}_{G,G'} = c^{12}_{G-G'}(\boldsymbol{k}+\boldsymbol{G})_1(\boldsymbol{k}+\boldsymbol{G}')_2 + c^{66}_{G-G'}(\boldsymbol{k}+\boldsymbol{G})_2(\boldsymbol{k}+\boldsymbol{G}')_1, \tag{A.4}$$

$$\boldsymbol{Q}^{(2,1)}_{G,G'} = c^{12}_{G-G'}(\boldsymbol{k}+\boldsymbol{G})_2(\boldsymbol{k}+\boldsymbol{G}')_1 + c^{66}_{G-G'}(\boldsymbol{k}+\boldsymbol{G})_1(\boldsymbol{k}+\boldsymbol{G}')_2, \tag{A.5}$$

$$\boldsymbol{Q}^{(2,2)}_{G,G'} = c^{11}_{G-G'}(\boldsymbol{k}+\boldsymbol{G})_2(\boldsymbol{k}+\boldsymbol{G}')_2 + c^{66}_{G-G'}(\boldsymbol{k}+\boldsymbol{G})_1(\boldsymbol{k}+\boldsymbol{G}')_1, \tag{A.6}$$

$$\boldsymbol{Q}^{(3,3)}_{G,G'} = c^{44}_{G-G'}(\boldsymbol{k}+\boldsymbol{G})_1(\boldsymbol{k}+\boldsymbol{G}')_1 + c^{44}_{G-G'}(\boldsymbol{k}+\boldsymbol{G})_2(\boldsymbol{k}+\boldsymbol{G}')_2, \tag{A.7}$$

$$\boldsymbol{Q}^{(3,4)}_{G,G'} = e^{15}_{G-G'}(\boldsymbol{k}+\boldsymbol{G})_1(\boldsymbol{k}+\boldsymbol{G}')_1 + e^{15}_{G-G'}(\boldsymbol{k}+\boldsymbol{G})_2(\boldsymbol{k}+\boldsymbol{G}')_2, \tag{A.8}$$

$$\boldsymbol{Q}^{(4,3)}_{G,G'} = \boldsymbol{Q}^{(3,4)}_{G,G'}, \tag{A.9}$$

$$\boldsymbol{Q}^{(4,4)}_{G,G'} = -\epsilon^{11}_{G-G'}(\boldsymbol{k}+\boldsymbol{G})_1(\boldsymbol{k}+\boldsymbol{G}')_1 - \epsilon^{11}_{G-G'}(\boldsymbol{k}+\boldsymbol{G})_2(\boldsymbol{k}+\boldsymbol{G}')_2. \tag{A.10}$$

References

[1] Sigalas M M and Economou E N 1993 Band structure of elastic waves in two dimensional systems *Solid State Commun.* **86** 141–3

[2] Kushwaha M S, Halevi P, Dobrzynski L and Djafari-Rouhani B 1993 Acoustic band structure of periodic elastic composites *Phys. Rev. Lett.* **71** 2022–5

[3] Liu Z, Chan C T, Sheng P, Goertzen A L and Page J H 2000 Elastic wave scattering by periodic structures of spherical objects: theory and experiment *Phys. Rev.* B **62** 2446–57

[4] Li X, Wu F, Hu H, Zhong S and Liu Y 2003 Large acoustic band gaps created by rotating square rods in two-dimensional periodic composites *J. Phys. D: Appl. Phys.* **36** L15–7

[5] Wilm M, Khelif A, Ballandras S, Laude V and Djafari-Rouhani B 2003 Out-of-plane propagation of elastic waves in two-dimensional phononic band-gap materials *Phys. Rev.* E **67** 065602

[6] Laude V, Wilm M, Benchabane S and Khelif A 2005 Full band gap for surface acoustic waves in a piezoelectric phononic crystal *Phys. Rev.* E **71** 036607

[7] Khelif A, Aoubiza B, Mohammadi S, Adibi A and Laude V 2006 Complete band gaps in two-dimensional phononic crystal slabs *Phys. Rev.* E **74** 046610

[8] Hou Z, Wu F and Liu Y 2004 Phononic crystals containing piezoelectric material *Solid State Commun.* **130** 745–9

[9] Wu T T, Hsu Z C and Huang Z G 2005 Band gaps and the electromechanical coupling coefficient of a surface acoustic wave in a two-dimensional piezoelectric phononic crystal *Phys. Rev.* B **71** 064303

[10] Li F M, Wang Y Z, Fang B and Wang Y S 2007 Propagation and localization of two-dimensional in-plane elastic waves in randomly disordered layered piezoelectric phononic crystals *Int. J. Solids Struct.* **44** 7444–56

[11] Li F M, Xu M Q and Wang Y S 2007 Frequency-dependent localization length of SH-wave in random disordered piezoelectric phononic crystals *Solid State Commun.* **141** 296–301

[12] Villeneuve P R and Piché M 1992 Photonic band gaps in two-dimensional square and hexagonal lattices *Phys. Rev.* B **46** 4969–72

[13] Villeneuve P R and Piché M 1992 Photonic band gaps in two-dimensional square lattices: square and circular rods *Phys. Rev.* B **46** 4973–5

[14] Villeneuve P R and Piché M 1991 Photonic band gaps of transverse electric modes in two-dimensional periodic media *J. Opt. Soc. Am.* A **8** 1296–305

[15] Wang R Z, Wang X H, Gu B Y and Yang G Z 2001 Effects of shapes and orientations of scatterers and lattice symmetries on the photonic band gap in two-dimensional photonic crystals *J. Appl. Phys.* **90** 4307–13

[16] Susa N 2002 Large absolute and polarization-independent photonic band gaps for various lattice structures and rod shapes *J. Appl. Phys.* **91** 3501–10

[17] Zhong L, Wu F, Zhang X, Zhong H and Zhong S 2005 Effects of orientation and symmetry of rods on the complete acoustic band gap in two-dimensional periodic solid/gas systems *Phys. Lett.* A **339** 164–70